VNU Journal of Science: Mathematics - Physics
Journal homepage: https://js.vnu.edu.vn/MaP

Original Article

Machine Learning-based Single-cell Analysis Using Microfluidic Impedance Flow Cytometer

Phan Hoang Anh[1], Nguyen Van Phu[2], Le Thanh Tung[1], Duong Van Tan[1], Dao Anh Phuc[2], Pham Van Dai[1], Do Quang Loc[2,*], Bui Thanh Tung[1], Chu Duc Trinh[1]

[1]*VNU University of Engineering and Technology, 144 Xuan Thuy, Cau Giay, Hanoi, Vietnam*
[2]*VNU University of Science, 334 Nguyen Trai, Thanh Xuan, Hanoi, Vietnam*

Received 27th December 2024
Revised 17th April 2025; Accepted 16th June 2025

Abstract: Single-cell analysis offers a more comprehensive approach to disease diagnosis compared to conventional methods. Electrical properties at a cellular level have been established as reliable biomarkers, enabling the identification of variations between individual cells. In this work we introduce a machine learning-based methodology for analyzing electrical impedance signals obtained from a microfluidic biosensor system for biological cell analysis. The proposed model is designed to detect and enumerate CD4 T-lymphocytes (CD4), which are a critical component of the immune system, through a microfluidic impedance flow cytometer. By identifying and analyzing the bioelectrical signal characteristics of CD4 cells as they traverse the sensing region, the machine learning models provide accurate cell enumeration while also estimating the size distribution of cell populations within the sample. A signal classification framework is employed to isolate cell signals from background noise, followed by the application and evaluation of various machine learning algorithms to optimize performance. The proposed method demonstrates improved accuracy and speed in cellular analysis compared to traditional techniques such as flow cytometry. Moreover, this method presents a significant potential for applications in cell analysis, addressing the demand for point-of-care diagnostics and enhancing the efficiency of biological diagnostics.

Keywords: Biosensor, impedance sensing, microfluidic, single-cell analysis, machine learning.

1. Introduction

Single-cell analysis has emerged as a crucial tool in modern disease diagnostics due to its ability to provide detailed information at the cellular level, enabling the detection and evaluation of biological

* Corresponding author.
E-mail address: locdq@vnu.edu.vn

https//doi.org/10.25073/2588-1124/vnumap.4984

features that are often inaccessible to traditional methods [1, 2]. However, existing techniques such as flow cytometry face significant limitations, including operational complexity, high costs, and challenges in scaling applications beyond specialized laboratory settings [3-6]. In this context, cellular electrical properties, such as impedance, have been established as reliable biomarkers, allowing precise differentiation between cells based on their physical and physiological characteristics. The advancement of microfluidic sensing systems, combined with electrical signal analysis, offers promising new directions to overcome the limitations of traditional methods while delivering efficient, cost-effective, and easily deployable solutions for practical applications.

While single-cell analysis holds significant potential, achieving high accuracy and efficiency in processing signals from individual cells remains a major challenge [7-9]. Electrical signals from single cells are typically weak and highly susceptible to background noise in microfluidic environments, reducing the reliability of measurement results [10-12]. This necessitates highly sensitive sensing systems and advanced signal processing methods to isolate meaningful signals from noise effectively. Furthermore, the pressing demand for rapid, cost-effective, and easily deployable diagnostic solutions at point-of-care settings is driving the development of innovative technologies [13]. These solutions must ensure high performance while being simple enough for widespread application, particularly in resource-limited settings with constrained infrastructure and manpower.

In recent years, impedance flow cytometry (IFC) has gained significant attention as a powerful label-free technique for analyzing individual cells based on their electrical properties. This approach allows for the characterization of cell size, morphology, and internal structure by measuring impedance changes as cells traverse a microfluidic channel [14-16]. Notable studies have developed microfluidic systems for applications such as cancer cell detection, immune cell counting, and the analysis of cellular physiological properties based on impedance signals [17-19]. For instance, systems employing microelectrodes for impedance measurement have shown promising results in tumor cell detection but are often limited by sensitivity and signal resolution [20]. These challenges, coupled with the complexity of processing impedance signals affected by substantial background noise, have driven the adoption of artificial intelligence (AI) as an effective solution for signal processing and biomedical diagnostics.

Cellular signal analysis relies on impedance values and complex features such as signal shape, frequency, and correlations between parameters. This complexity makes machine learning methods highly advantageous, given their ability to handle multidimensional data and extract deeper insights from signals. Several studies have successfully applied machine learning and deep learning to single-cell analysis [21, 22]. Wei et al., [23] utilized machine learning to classify cellular states based on impedance features obtained from impedance flow cytometry (IFC). Their research demonstrated significant potential for label-free single-cell analysis, achieving near-perfect accuracy in distinguishing live and dead cell states and drug-inhibited states in cancer cell lines such as H1650 and HeLa. Honrado et al., [24] developed a neural network-based approach for the real-time characterization of particles and cells using impedance data from microfluidic cytometry. Their method accurately determined the size, velocity, and cross-sectional position of particles, red blood cells, and yeast with a processing time of only 0.4 ms, highlighting its promise for real-time single-cell analysis and sorting. Machine learning and deep learning algorithms have also been employed to classify cancer cells based on impedance signals, while other models have successfully detected differences in the size and state of immune cells [25]. Despite these advancements, there remain challenges in improving accuracy and enabling practical deployment. This underscores a significant opportunity to integrate AI with microfluidic sensing systems to optimize performance and expand their application in biomedical diagnostics.

This study presents the development of a machine learning-based framework for analyzing impedance signals from single cells using a microfluidic sensor system. A custom-designed microfluidic biochip was fabricated to detect and enumerate CD4 T-lymphocytes (CD4 T cells) through impedance

measurements, incorporating a cost-efficient signal processing circuit that includes an instrumental amplifier and a highly sensitive lock-in amplifier. The primary objective is to accurately detect and count CD4 T cells, a key component of the immune system, to support immune health monitoring and disease diagnosis. The proposed framework employs a systematic multi-step methodology for signal processing. A segmentation model is initially utilized to identify and isolate cell-specific signal segments from the raw impedance data. Subsequently, critical bioelectrical features are extracted and characterized to facilitate analysis. By exploiting these features, the framework enables precise cell enumeration and estimates the size distribution of cell populations within the sample. The framework then evaluates multiple machine learning models to identify the optimal classifier for signal interpretation, with results demonstrating high accuracy and recall, underscoring the robustness of the approach. This methodology represents a non-invasive, efficient, and scalable solution tailored to precision medicine and single-cell analysis demands. Integrating microfluidic impedance sensing with machine learning addresses critical challenges in modern biomedical diagnostics, offering a versatile platform for advanced healthcare applications.

2. Materials and Methods

2.1. Cell Detection Using a Microfluidic Chip and Compact Signal Processing Circuit

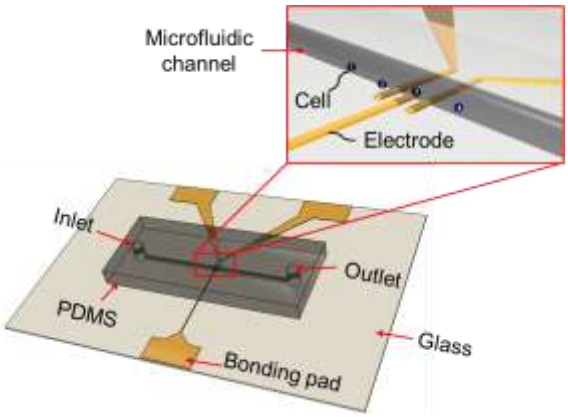

Figure 1. Design of a microfluidic IFC for CD4 T cell analysis with excitation and pick-up electrode configuration.

Figure 1 illustrates the design of a microfluidic chip developed for detecting and enumerating biological cells using a single microfluidic channel. The sensing structure comprises three coplanar metal electrodes, one excitation electrode positioned centrally and two pick-up electrodes on either side, fabricated using microfabrication technology. The differential signal between the two pick-up electrodes indicates the movement of cells within the fluidic channel, while the impedance values of the central excitation electrode and the adjacent sensing electrodes are analyzed to measure variations at each cell position as it traverses the channel. The presence of viable cells is determined based on the impedance imbalance between the adjacent sensing electrode pairs. A wheatstone bridge circuit is employed to detect relative impedance changes, and the output signals from the two pick-up electrodes are differentially amplified before being processed by a lock-in amplifier to suppress background noise. The previous study performed detailed simulations of impedance variations within the sensing region [26]. The fabricated chip was integrated with a signal processing circuit to conduct experiments for detecting and counting CD4 T cells within the microfluidic channel.

The microfluidic chip was fabricated by integrating a glass substrate with impedance-detecting electrodes and a PDMS microfluidic channel layer. The electrodes were created using metal deposition, photolithography, and wet etching, with 20 nm of chromium and 100 nm of gold deposited onto the glass substrate after cleaning with piranha solution. The microfluidic channel was fabricated using soft lithography, where Polydimethylsiloxane (PDMS, Sylgard-184 Silicone Elastomer Kit, Dow Corning, Midland, MI, USA) (10:1 is the ratio of prepolymer to curing agent) was poured into an SU-8 mold (MicroChem Corp., Newton, MA, USA), degassed under vacuum, baked at 65 °C, and punched to create inlet and outlet ports. The PDMS layer was bonded to the glass substrate using oxygen plasma treatment, and the assembled chip was baked at 90 °C to complete the fabrication process.

CD4 T cells were used to evaluate the chip's performance and the signal processing circuit. Peripheral blood mononuclear cells (PBMCs) were isolated from diluted blood using Pancoll gradient centrifugation, cleaned, and labeled with FC-CD4 before magnetic separation to collect labeled cells (positive fraction). The signal processing circuit was compactly designed to handle sinusoidal signals of 1 Vp-p at 100 kHz applied to the excitation electrode. Signals from the pick-up electrodes were amplified and processed through a Wheatstone bridge, an INA111 (Texas Instruments) instrumentation amplifier, and an AD630 (Analog Devices) demodulator to suppress noise. The processed signal was filtered through a low-pass filter and buffered before being transmitted to an Arduino Mega microcontroller, followed by the data acquisition.

2.2. Data Acquisition from Microfluidic Device

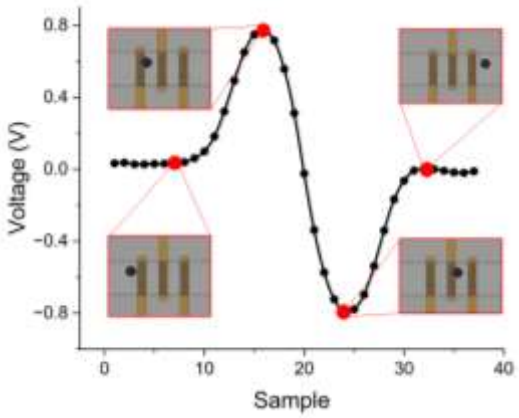

Figure 2. Variation of output signals with the passage of CD4 T cells over the counting region. The insets in the graph indicate the positions of the cell corresponding to the output voltage at each point.

The electrical signals generated by the movement of CD4 T cells through the sensing region were collected, processed, and analyzed. The passage of the cells caused a time-dependent variation in the output signal. Figure 2 illustrates the measured voltage changes as a CD4 T cell traverses the electrodes. The inset images show the cell's position at different locations corresponding to specific points on the voltage trace. The recorded signal exhibits bipolar peaks, resulting from the cell passing over both pairs of sensing electrodes. Positive polarity peaks occur as the cell moves across the first pair of electrodes, while negative peaks are observed as it crosses the second pair. The baseline voltage, approximately 0.14 V, represents the offset voltage when no cell is present in the sensing region. This offset voltage may be attributed to electrode fabrication imperfections or the precision limitations of the electronic components. The signal profile indicates that the positive peaks demonstrate a higher amplitude than the negative ones. The maximum voltage deviations from the baseline were measured to be approximately

1.4 V for the positive peaks and 1.7 V for the negative peaks. This amplitude disparity is likely caused by hydrodynamic forces exerted on the cell as it traverses the electrode region, which may affect its relative vertical position within the microfluidic channel.

2.3. Cell Signal Segmentation from Data

In the time-discrete signal array collected from the microfluidic device, the segmentation and classification of cell signals are essential to differentiate them from noise. In previous studies, cell counting was implemented by evaluating the amplitude of the positive peaks against a fixed threshold. However, this approach has significant limitations when the data contains high-amplitude noise that exceeds the predefined threshold. Moreover, the unique signal shape, which consists of consecutive positive and negative peaks (Figure 3), can be leveraged as a distinct feature to detect and count cells passing through the electrodes more accurately. For each cell signal within the collected data array, key reference points are defined: Start Point (SP), End Point (EP), Positive Peak (PP), and Negative

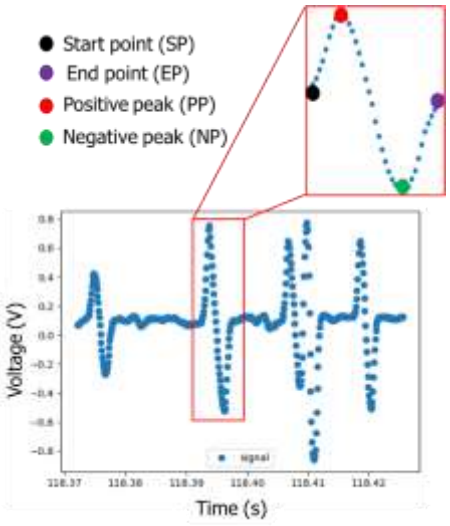

Figure 3. Definition of cell signal segments in the data array. Each signal is characterized by a Start Point (SP), an End Point (EP), a Positive Peak (PP), and a Negative Peak (NP).

Peak (NP). To construct this 2D signal segmentation model, specific conditions are established as follows: the voltage values of SP and EP must remain below the baseline (where the baseline is defined as the signal when the voltage value is approximately 0), the heights of PP and NP are required to be similar, and any waveforms that deviate noticeably from a bipolar shape are classified as noise. This refined approach improves the accuracy of cell detection and enumeration accuracy while addressing previous methods' limitations in noisy environments.

The signal identification and extraction process are conducted in two main steps. The identification of positive peaks (PP) and negative peaks (NP) is performed using the find peaks function (detects local maxima in the signal data) from the scipy library, specifically designed for peak detection in signal data. Specifically, the PPs are detected directly, while the NPs are determined by inverting the input parameter’s sign in the method. Once the PPs and NPs are collected, their number is reduced by removing identifiable noise peaks. The remaining PPs and NPs are then balanced in quantity and paired accordingly. These PP-NP pairs determine the Start Point (SP) and End Point (EP) of the signals. The SP is identified by tracing backward from the PP's position until the voltage's decreasing trend ends. Similarly, the EP is located by tracing forward from the NP until the increasing trend ceases. Finally, all

data points from SP to EP are grouped into a vector, and the process is repeated until no PP-NP pairs remain. Figure 4 illustrates the workflow, including peak detection, SP and EP identification, and final signal extraction after noise removal.

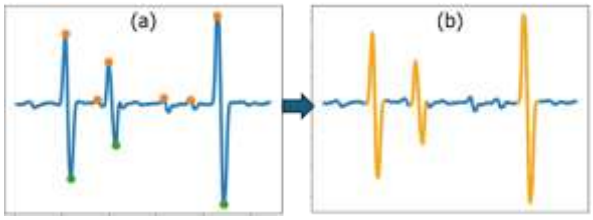

Figure 4. Cell signal segmentation process: (a) Find definition peaks from the entire signal; (b) Segmentation the cell signal.

2.4. Feature Description for Machine Learning Models

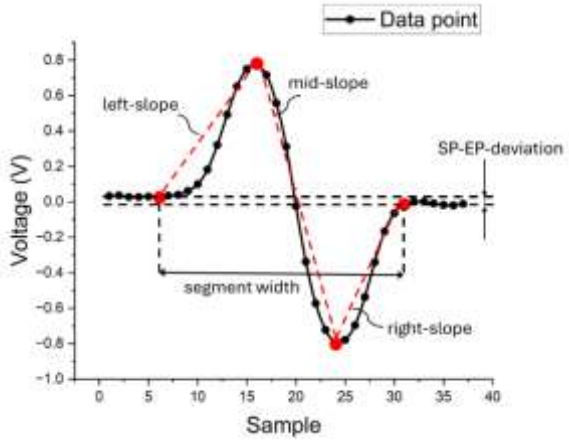

Figure 5. The definition of features including: segment-width (horizontal distance between Start Point and End Point); SP-EP-deviation (vertical distance between SP and EP); Standard Deviation (SD) of the data points; left-slope, mid-slope, and right-slope quantify the peak's slope angles.

The preprocessing procedure filters out signal segments with peak patterns resembling those generated by CD4-T cells. However, the segmentation model primarily eliminates background noise and measurement circuit interference. In practice, CD4-T cells are not the only entities passing through the electrodes and producing such signal patterns. The sample may also contain cell debris, cell clusters, dust particles, or other impurities, which can generate electrical signals with similar shapes. Despite this overlap, each type of object in the sample exhibits distinct signal characteristics that can be leveraged for further classification. Since most detected objects are cells, specific signal features can be defined. Machine learning models can be applied to accurately determine whether a given signal corresponds to a cell if it lies within the defined convergence region. This approach enhances the reliability of identifying CD4-T cell signals while reducing false positives caused by non-cellular artifacts.

In this study, signal features were defined and evaluated using over 1,000,000 data points collected from experiments. The segment width represents the distance between the SP and the EP and provides critical information about the duration of the signal in terms of time samples. The SP-EP deviation quantifies the voltage difference between SP and EP and serves as another key indicator. The discrete signal segment is also analyzed for smoothness to ensure its validity. Any anomalies or outliers that

cause a significant increase in the standard deviation (SD) of the segment are not considered valid cell signals. The slope angles are calcula

Machine Lea ted as left-slope for SP-to-PP, mid-slope for PP-to-NP, and right-slope for NP-to-EP to capture the signal's shape. These features are illustrated in Figure 5. Most signal instances filtered from the raw data exhibit similar patterns for the defined features.

2.5. Implementation of rning Models

After defining and extracting the relevant features from the entire dataset, the data were applied to several widely used machine learning classification models to compare and evaluate their performance. The data used for training consists of two classes: the majority class, representing instances labeled as actual cell signals, and the minority class, representing instances labeled as noise. This study proposes two approaches for training the machine learning models: one-class classification and binary classification. For the one-class classification approach, models such as Isolation Forest and One-Class SVM are utilized to identify and isolate cell signal instances without explicitly relying on noise labels. In contrast, the two-class classification approach employs widely used models, including Decision Tree, Random Forest, Logistic Regression, Support Vector Classifier (SVC), K-Neighbors Classifier, and Gradient Boosting Classifier, to differentiate between cell signals and noise instances. The comparative analysis between these two training strategies evaluates their effectiveness in handling imbalanced datasets and improving the accuracy of cell signal detection in microfluidic systems.

3. Results and Discussion

Four standard metrics were employed to evaluate the performance of the machine learning models used in this work: Accuracy, Precision, Recall, and F1-score. These metrics comprehensively assess each model's ability to distinguish between actual cell signals and noise.

Accuracy measures the overall correctness of the model and is defined as:

$$Accuracy = \frac{TP + TN}{TP + TN + FP + FN}$$

Where TP is True Positive, TN is True Negative, FP is False Positive, and FN is False Negative.

Precision reflects the proportion of predicted positive instances that are correct, capturing the model's reliability:

$$Precision = \frac{TP}{TP + FP}$$

Recall (or Sensitivity) measures the model's ability to identify all relevant instances of the positive class correctly:

$$Recall = \frac{TP}{TP + FN}$$

F1-Score is the harmonic mean of Precision and Recall, providing a balanced measure when dealing with imbalanced datasets:

$$F1 - Score = 2 \times \frac{Precision \times Recall}{Precision + Recall}$$

By applying these metrics, the study ensures a thorough evaluation of the machine learning models' performance across both one-class and two-class classification approaches. Accuracy highlights overall correctness, while Precision and Recall provide insights into false positives and false negatives, respectively. F1-score is a balanced metric, particularly valuable for imbalanced datasets like the one used in this research.

3.1. Data Acquisition and Segmentation Model Performance

The dataset utilized in this study comprised over 1,000,000 data points collected from experimental recordings, which were segmented into a total of 1,473 labeled instances for training and testing purposes. To rigorously evaluate the performance and generalizability of the machine learning models, a stratified 5-fold cross-validation technique was employed. Specifically, the dataset was partitioned into five subsets of equal size, ensuring balanced representation of cell and non-cell signals in each subset. In each iteration, four subsets were used for model training, while the remaining subset served as the validation set, with this process repeated five times. The final performance metrics, including accuracy, precision, recall, and F1-score, were calculated as averages across these five folds. Statistical significance of model differences was assessed using paired t-tests, with a significance threshold set at $p < 0.05$. The segmentation model achieved a Precision of 85.33% and a Recall of 96.76% on this dataset. The results indicate that the segmentation step effectively captures most cell signals while minimizing false positives. Further analysis revealed that most instances missed during this stage have minimal peak voltage values of approximately 0.1 V. These findings highlight the model's strong performance while underscoring the challenge of accurately identifying signals with minimal voltage variation.

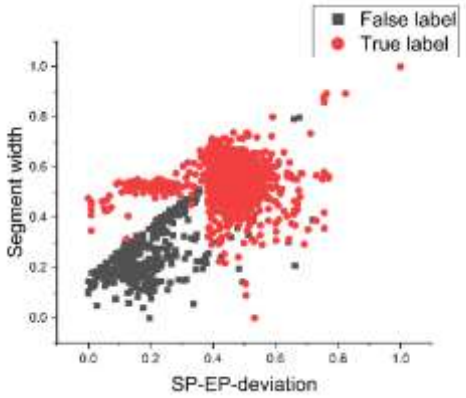

Figure 6. The convergence and distinction between the two features, segment width and SP-EP-deviation, for cell-labeled data and non-cell-labeled data.

3.2. Features Evaluation

The scatter plot in Figure 6 illustrates the distribution and distinction between two key features, segment width and SP-EP-deviation, for previously labeled data points representing cell signals (true labels) and non-cell signals (false labels). The plot demonstrates a clear clustering pattern, where the actual cell signals predominantly occupy regions with moderate values of SP-EP-deviation and segment width. In contrast, the non-cell signals exhibit greater dispersion, primarily concentrated in areas with lower values of these two features. This result highlights the effectiveness of segment width and SP-EP-deviation in distinguishing between cell signals and background noise. The convergence observed for these features indicates their strong potential for signal classification tasks. Similar patterns of convergence are also evident in other extracted features. The following section will present the classification results using both one-class and two-class machine learning models.

3.3. Classification Model Performance

The performance of the one-class classification models, presented in Table I, demonstrates that IsolationForest achieves the highest Accuracy of 0.882. However, OneClassSVM outperforms it in

Precision (0.785) and Recall (0.795), resulting in a higher F1-score of 0.790 compared to 0.720 for IsolationForest. This result suggests that while IsolationForest captures a broader set of instances, it may include more false positives, as indicated by its lower Precision. Conversely, OneClassSVM demonstrates a better balance between correctly identifying cell signals and reducing noise, making it more reliable for this dataset. Nevertheless, the overall performance of the one-class models remains suboptimal, which may be attributed to the insufficient convergence of the defined features. The limited distinction between actual cell signals and noise could hinder the clustering models' ability to classify the signals accurately.

Table 1. One-Class model performance

Model	Accuracy	Precision	Recall	F1-score
IsolationForest	0.882	0.715	0.735	0.720
OneClassSVM	0.842	0.785	0.795	0.790

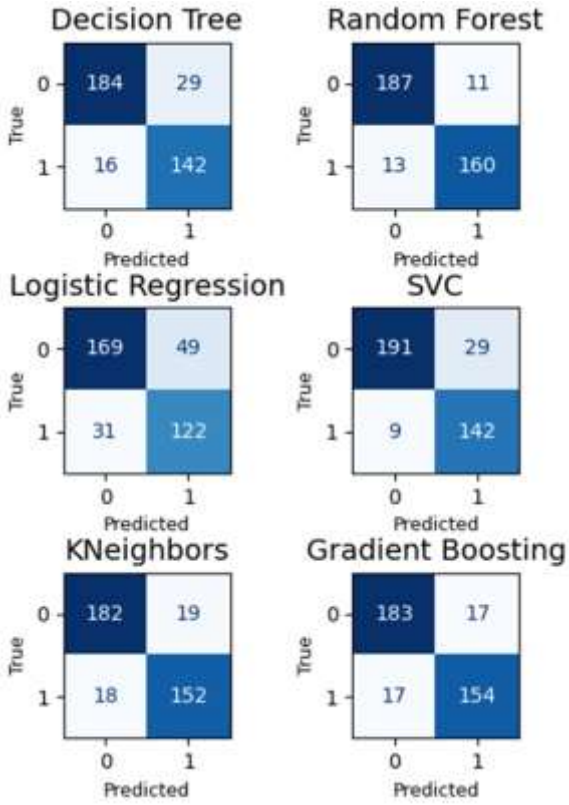

Figure 7. Confusion matrix of 6 classification models.

For the evaluation of classification machine learning models, the labeled dataset was divided into a training set and a testing set, with the model performance on the testing set summarized through confusion matrices (Figure 7). The confusion matrices provide a comprehensive overview of the performance of six machine learning models: Decision Tree, Random Forest, Logistic Regression, SVC, KNeighbors Classifier, and Gradient Boosting in the two-classes classification task. Ensemble-based methods, such as Random Forest and Gradient Boosting, along with SVC, demonstrated superior performance with fewer misclassifications than the other models. In contrast, Logistic Regression and

Decision Tree exhibited higher misclassification rates, reflecting their limitations in capturing the complex features of the signal data. The KNeighbors achieved competitive results, showing consistent performance across both classes.

To further evaluate the models, the metrics accuracy, precision, recall, and F1-score were calculated (Table 2). KNeighbors and Gradient Boosting achieved the highest overall performance, with Accuracy values of 0.896 and 0.895, respectively. Both models demonstrated exceptional Recall (0.918 for KNeighbors and 0.903 for Gradient Boosting), making them highly effective in identifying actual cell signals. The F1-score for KNeighbors (0.896) slightly exceeds that of Gradient Boosting (0.895), highlighting its robustness in balancing Precision and Recall. Notably, the Random Forest model exhibited the highest Precision (0.908) but slightly lower Recall, indicating that it is particularly effective at minimizing false positives. Overall, these results suggest that the two-class classification approach, mainly using KNeighbors and Gradient Boosting, outperforms the one-class models in terms of accuracy and reliability, making it a preferred choice for this dataset.

Table 2. Two-Classes model performance

Model	Accuracy	Precision	Recall	F1-score
Decision Tree	0.808	0.812	0.855	0.833
Random Forest	0.870	**0.908**	0.855	0.881
Logistic Regression	0.743	0.748	0.817	0.781
SVC	0.873	0.864	**0.918**	0.890
Kneighbors	**0.881**	0.876	**0.918**	**0.896**
Gradient Boosting	**0.881**	0.886	0.903	**0.895**

Although various classifiers were evaluated in this study, providing a clear justification for selecting the final model would enhance the persuasiveness of the research findings. Based on the performance metrics obtained, the two-class classification method, despite requiring extensive labeled data and supervised training, consistently demonstrated superior performance in terms of accuracy, precision, recall, and F1-score compared to the one-class classification method. Among the evaluated two-class models, KNeighbors emerged as the most effective classifier, achieving the highest accuracy and F1-score. This indicates its balanced capability in classification precision and the accurate identification of actual cell signals. Therefore, the selection of the KNeighbors model is not solely justified by quantitative metrics but also by its practical efficacy, thereby enhancing both the reliability and applicability of the research outcomes.

3.4. Characteristics of Cell

The scatter plot in Figure 8 illustrates the distribution of two key signal features: segment width, which represents the signal duration, and the PP-NP ratio, which reflects the amplitude ratio between the positive and negative peaks. These features provide critical insights into the size and distribution of the cell population within the sample. Most data points are concentrated in regions with moderate segment width values and low PP-NP ratios, indicating that most cells in the population exhibit similar sizes and relatively balanced signal peaks. However, a subset of data points with higher PP-NP ratios and varying segment widths suggests the presence of larger cells or cells positioned unevenly relative to the electrodes. This distribution highlights the heterogeneity within the cell population and the ability of these features to differentiate unique cells based on their signal characteristics, thereby enhancing the accuracy of single-cell analysis.

It would be beneficial to consider comparative studies involving deep learning models, such as Convolutional Neural Networks (CNNs) and Long Short-Term Memory networks (LSTMs), for

recognizing distinct cellular characteristics within the same population. Given the capability of deep learning approaches to capture intricate, high-dimensional patterns in sequential and spatial data, employing CNNs or LSTMs may offer enhanced accuracy and deeper insights into the subtle variations among cells that traditional machine learning models might not fully capture. This comparative evaluation could further establish robust methodologies for single-cell analysis, potentially uncovering new biomarkers and improving diagnostic precision in complex biological systems.

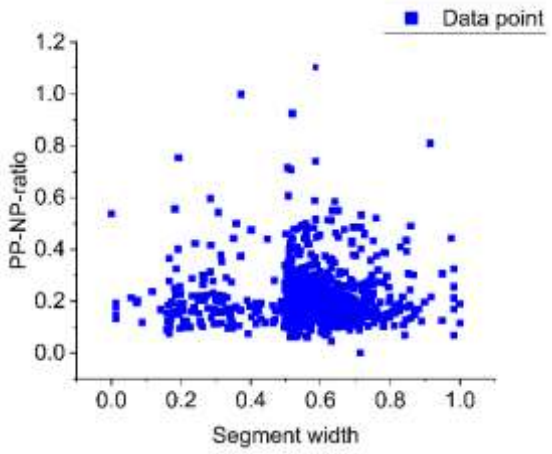

Figure 8. The distribution of cell signal segment width and the ratio of the positive peak to the negative peak.

4. Conclusions

This study developed a framework integrating microfluidic impedance sensing and machine learning to detect and enumerate CD4 T-lymphocytes accurately. A custom-designed bio-microfluidic chip, combined with a cost-effective signal processing circuit and a highly sensitive amplifier, enabled the extraction and analysis of key bioelectrical features. The system demonstrated a high accuracy in cell counting and provided reliable estimates of the size distribution within cell populations, as validated by evaluating machine learning models. The obtained results confirm the effectiveness and scalability of the proposed approach, highlighting its significant potential for applications in precision medicine and modern single-cell analysis.

Acknowledgments

This work was funded by the Vietnam Ministry of Science and Technology under Grant DTDL.CN-40/23.

References

[1] T. Sun, H. Morgan, Single-cell Microfluidic Impedance Cytometry: A Review, Microfluid Nanofluidics, Vol. 8, No. 4, 2010, pp. 423-443, https//doi.org/1007/S10404-010-0580-9.
[2] C. Petchakup et al., Advances in Single Cell Impedance Cytometry for Biomedical Applications, Micromachines Vol. 8, No. 3, 2017, pp. 87, https//doi.org/10.3390/MI8030087.
[3] K. Cheung, S. Gawad, P. Renaud, Impedance Spectroscopy Flow Cytometry: On-chip Label-Free Cell Differentiation, Cytometry A, Vol. 65, No. 2, 2005, pp. 124-132, https//doi.org/10.1002/CYTO.A.20141.
[4] M. E. Piyasena S. W. Graves, The Intersection of Flow Cytometry with Microfluidics Microfabrication, Lab Chip, Vol. 14, No. 6,2014, pp. 1044-1059, https//doi.org/10.1039/C3LC51152A.

[5] D. R. Gossett et al., Label-Free Cell Separation Sorting in Microfluidic Systems, Anal Bioanal Chem, Vol. 397, No. 8, 2010, pp. 3249-3267, https//doi.org/10.1007/S00216-010-3721-9.
[6] J. Chen, C. Xue, Y. Zhao, D. Chen, M. H. Wu, J. Wang, Microfluidic Impedance Flow Cytometry Enabling High-Throughput Single-Cell Electrical Property Characterization, International Journal of Molecular Sciences 2015, Vol. 16, No. 5, 2015, pp. 9804-9830, https//doi.org/10.3390/Ijms16059804.
[7] S. Kumari et al., Microfluidic Platforms for Single Cell Analysis: Applications in Cellular Manipulation Optical Biosensing, Chemosensors 2023, Vol. 11, No. 2, 2023, pp. 107, https//doi.org/10.3390/Chemosensors11020107.
[8] Y. Manmana, K. Yamada, D. Citterio, Paper-Based Microfluidics for Point-of-care Medical Diagnostics, 2024, pp. 443-493, https//doi.org/10.1007/978-981-97-6540-9_13.
[9] C. Honrado, P. Bisegna, N. S. Swami, F. Caselli, Single-Cell Microfluidic Impedance Cytometry: from Raw Signals to Cell Phenotypes Using Data Analytics, Lab Chip, Vol. 21, No. 1, 2021, pp. 22-54, https//doi.org/10.1039/D0lc00840k.
[10] D. Vloemans, L. V.an Hileghem, H. Ordutowski, F. D. Dosso, D. Spasic, J. Lammertyn, Self-Powered Microfluidics for Point-Of-Care Solutions: from Sampling to Detection of Proteins Nucleic Acids, Methods Mol Biol, Vol. 2804, 2024, pp. 3-50, https//doi.org/10.1007/978-1-0716-3850-7_1.
[11] S. A. Graham, E. Segal, Lab-on-a-chip Devices for Point-of-care Medical Diagnostics, Adv Biochem Eng Biotechnol, Vol. 179, 2022, pp. 247-265, https//doi.org/10.1007/10_2020_127/Figures/9.
[12] F. Piorino, A. T. Patterson, M. P. Styczynski, Low-cost, Point-of-care Biomarker Quantification, Curr Opin Biotechnol, Vol. 76, 2022, pp. 102738, https//doi.org/10.1016/J.Copbio.2022.102738.
[13] A. McDavid et al., Data Exploration, Quality Control and Testing in Single-cell Qpcr-based Gene Expression Experiments, Bioinformatics, Vol. 29, No. 4, 2013, pp. 461-467, https//doi.org/10.1093/Bioinformatics/Bts714.
[14] J. Chen, C. Xue, Y. Zhao, D. Chen, M. H. Wu, J. Wang, Microfluidic Impedance Flow Cytometry Enabling High-Throughput Single-Cell Electrical Property Characterization, International Journal of Molecular Sciences Vol. 16, No. 5, 2015, pp. 9804-9830, https//doi.org/10.3390/IJMS16059804.
[15] K. Cheung, S. Gawad, and P. Renaud, Impedance Spectroscopy Flow Cytometry: On-chip Label-free Cell Differentiation, Cytometry Part A, Vol. 65A, No. 2, 2005, pp. 124-132, https//doi.org/10.1002/CYTO.A.20141.
[16] K. C. Cheung et al., Microfluidic Impedance-based Flow Cytometry, Cytometry Part A, Vol. 77A, No. 7, 2010, pp. 648-666, https//doi.org/10.1002/CYTO.A.20910.
[17] C. Honrado, P. Bisegna, N. S. Swami, F. Caselli, Single-cell Microfluidic Impedance Cytometry: from Raw Signals to Cell Phenotypes Using Data Analytics, Lab Chip, Vol. 21, No. 1, 2021, pp. 22-54, https//doi.org/10.1039/D0LC00840K.
[18] T. Sun, H. Morgan, Single-cell Microfluidic Impedance Cytometry: A Review, Microfluid Nanofluidics, Vol. 8, No. 4, 2010, pp. 423-443, https//doi.org/10.1007/S10404-010-0580-9/Tables/1.
[19] G. Wu et al., Optimizing Microfluidic Impedance Cytometry by Bypass Electrode Layout Design, Biosensors (Basel), Vol. 14, No. 4, 2024, pp. 204, https//doi.org/10.3390/Bios14040204/S1.
[20] T. A. Nguyen, T. I. Yin, G. Urban, A Cell Impedance Sensor Chip for Cancer Cells Detection with Single Cell Resolution, Proceedings of Ieee Sensors, 2013, https//doi.org/10.1109/Icsens.2013.6688160.
[21] C. Ferguson, Y. Zhang, C. Palego, X. Cheng, Recent Approaches to Design and Analysis of Electrical Impedance Systems for Single Cells Using Machine Learning, Sensors, Vol. 23, No. 13, 2023, pp. 5990, https//doi.org/10.3390/S23135990.
[22] Z. Gao, Y. Li, Enhancing Single-cell Biology Through Advanced AI-powered Microfluidics, Biomicrofluidics, Vol. 17, No. 5, 2023, https//doi.org/10.1063/5.0170050/2914114.
[23] J. Wei et al., Machine Learning Classification of Cellular States Based on the Impedance Features Derived from Microfluidic Single-cell Impedance Flow Cytometry, Biomicrofluidics, Vol. 18, No. 1, 2024, https//doi.org/10.1063/5.0181287/3061531.
[24] C. Honrado, J. S. McGrath, R. Reale, P. Bisegna, N. S. Swami, F. Caselli, A Neural Network Approach for Real-Time Particle/Cell Characterization in Microfluidic Impedance Cytometry, Anal Bioanal Chem, Vol. 412, No. 16, 2020, pp. 3835-3845, https//doi.org/10.1007/S00216-020-02497-9/Figures/5.
[25] J. Wei et al., Machine Learning Classification of Cellular States Based on the Impedance Features Derived From Microfluidic Single-cell Impedance Flow Cytometry, Biomicrofluidics, Vol. 18, No. 1, 2024, https//doi.org/10.1063/5.0181287/3061531.
[26] P. T. Huong et al., A Novel Approach to Detect CD4 T-Lymphocytes Using a Microfluidic Chip and Compact Signal Processing Circuit, 2024, https//doi.org/10.21203/RS.3.RS-5171054/V1.